Water Freezes at Near-zero Temperatures Using Carbon Nanotube Based Electrodes under Static Electric Fields

Zhi Huang[1], Sumanjeet Kaur[1,*], Musahid Ahmed[2] and Ravi Prasher[1,3,*]

[1]Energy Storage and Distributed Resources Division, Lawrence Berkeley National Laboratory, Berkeley, CA, USA.

[2]Chemical Sciences Division, Lawrence Berkeley National Laboratory, Berkeley, CA, USA.

[3]Department of Mechanical Engineeing, University of California, Berkeley, Berkeley, CA, USA.

*Corresponding to skaur1@lbl.gov and rsprasher@lbl.gov.

ABSTRACT

While static electric fields have been effective in controlling ice nucleation, the highest freezing temperature (T_f) of water that can be achieved in an electric field (E) is still uncertain. We performed a systematic study of the effect of an electric field on water freezing by varying the thickness of a dielectric layer and the voltage across it in an electro-wetting system. Results show that T_f first increases sharply with E, and then reaches a saturation at -3.5 °C after a critical value E of 6×10^6 V/m. Using classical heterogeneous nucleation theory, it is revealed that this behavior is due to saturation in the contact angle of the ice embryo with the underlying substrate. Finally, we show that it is possible to overcome this freezing saturation by controlling the uniformity of the electric field using carbon nanotubes. We achieve a T_f of -0.6 °C using carbon nanotubes based electrodes with an E of 3×10^7 V/m. This work sheds new light on the control of ice nucleation and has the potential to impact many applications ranging from food freezing to ice-production.

Key words: Electro freezing, interfaces, carbon nanotube, supercooling, freezing temperature, freezing saturation, heterogeneous nucleation

INTRODUCTION

Water freezing is important in the natural world pertaining to climate change, sea level change and survival of polar wildlife. It is also crucially relevant in many industrial applications including anti-icing [1-3] of aerodynamic surfaces and power transmission lines, ice production for cold thermal storage [4-5], fast food [6] and freezing desalination [7]. While effective control of ice nucleation (nucleation temperature, nucleation rate and ice crystal size, etc.) under different environmental conditions is highly desirable [8-11], in reality it has proven to be incredibly challenging. This is partly because water does not usually freeze at its equilibrium melting point but has significant supercooling [12-14] which has a profound impact on energy consumption. In addition, supercooling puts water in a metastable state [15-16] making it difficult to predict its behavior and hence control for various applications listed above.

Nucleation agents, mechanical vibrations, sinusoidal electric current and static electric field have been investigated to overcome supercooling [6, 17]. Nucleating agents are the most widely used, however disadvantages include liquid pollution and transport pipeline blockage due to particle agglomeration [18-19]. Other techniques to control supercooling have been mostly investigated on small water volumes with varying degrees of success. While theory and simulation have shown that the use of static electric field as promising for nucleation and supercooling control [20-22], the experimental evidence is mostly limited to small water droplets (< 20 μl). This makes it difficult to extrapolate its effectiveness for bulk water as shape (geometry) of water droplet also influences supercooling [23-24]. To the best of our knowledge, there are only a few publications on thin films of water (planar geometry that resembles bulk water), however the electric field strength (E) was limited to 1×10^6 V/m and the highest freezing temperature (T_f) reported was -5.68 °C [25-26]. However, the answer to two important questions is still unknown: what range of E can affect supercooling and is it possible to freeze water at 0 °C under high E?

Herein, we report the effect of electric field on ice nucleation (freezing temperature) through systematic control of the strength of the external electric field, which was achieved via applying voltages across a dielectric layer in an electro-wetting system [27]. As reported by others [25-26, 28], we also observed that supercooling decreased (or T_f increased) sharply with the E, however we observed that there is critical electric field strength (E_c) above which the increase in the strength of the electric field has diminishing returns. We provide a mechanistic understanding of this freezing saturation behavior using a simple heterogeneous ice nucleation model. Finally, we also show that by controlling the distribution of electric field using carbon nanotubes (CNT), E_c can be increased and near zero (T_f = -0.6 °C) can be achieved.

RESULTS AND DISCUSSION

Since nucleation is stochastic [29-31] and easily affected by many factors, a statistical method is required to measure the freezing temperatures [32-33]. Freezing properties were investigated by an experimental platform typically used for studies of electro-wetting [27], details of which are provided in the **Experimental Procedures** section. Briefly deionized water was contained in a PDMS coated aluminum cup where thickness (d) of PDMS was 20 μm (see details in **Experimental Procedures**). An aluminum cup worked as one of the electrodes and the other electrode was a thin metal wire that was immersed in water. For electro freezing studies, voltage (U) was applied between these electrodes as shown in **Figure 1a** and **b**. As the electric resistivity of PDMS (4 x 10^{13} ohm-m) is approx. 6 orders of magnitude higher than that of DI water (2 x 10^7 ohm-m), the major voltage drop is across the PDMS layer. Under this situation, there is a strong electric field across the dielectric layer of PDMS (**Figure 1b**), the strength of which is given by $E = U / d$. The advantage of the electro-wetting setup is that the dielectric layer (PDMS) prevents both current flow and voltage drop across the liquid, thus electro-

freezing effects can be solely attributed to the near-surface electric field [24, 28].

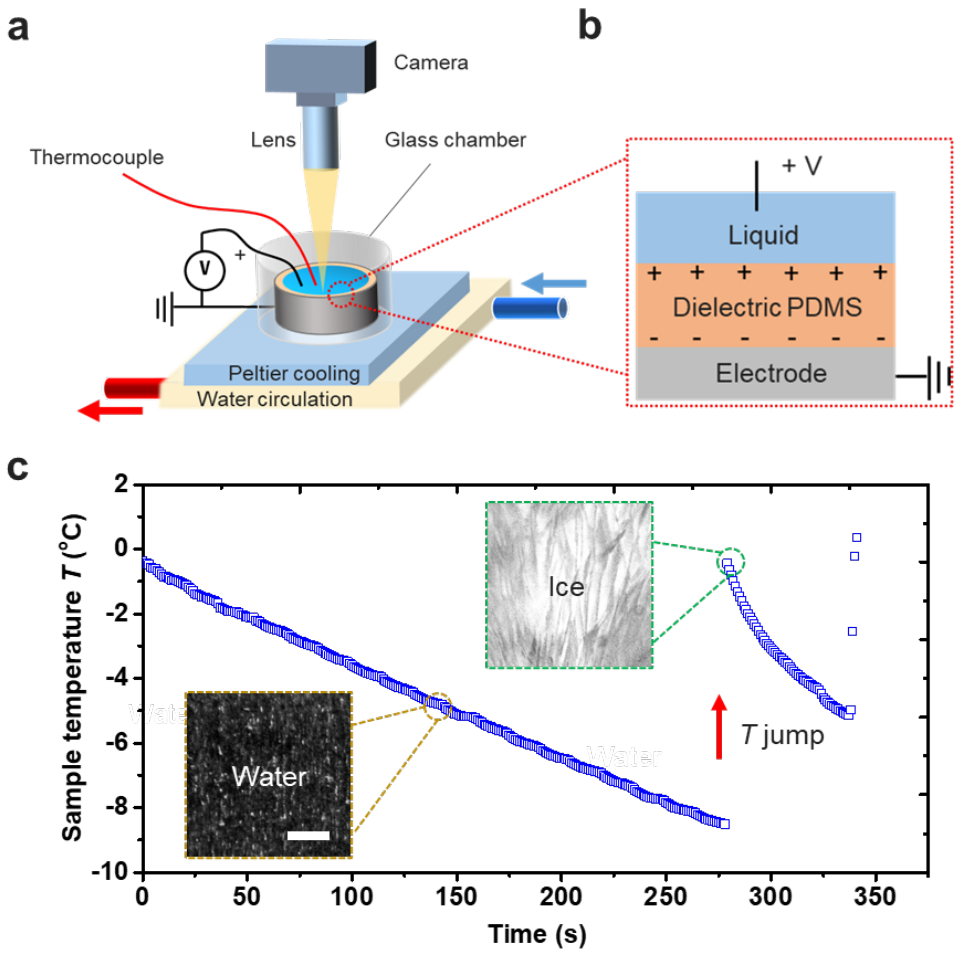

Figure 1. Electro-freezing setup and experimental data acquisition. *(a) Schematic of the setup used for electro-freezing experiments where the deionized water was contained in a PDMS coated aluminum cup. A wire was immersed in the deionized water and the voltage was applied across the wire and the aluminum cup, which resulted in a strong electric field E across the dielectric layer of PDMS as shown in (b). The optical camera was used only to capture the solid and liquid phases as shown as insets in Figure 1c, and was not used to determine the freezing temperature. (c) Temperature-time curve showing the onset of freezing. The temperature of the water was decreased linearly at the rate of 2 °C* min^{-1} *until there was a sudden temperature jump to 0 °C due to the release of latent heat. The point just before the sudden jump in temperature was taken as the freezing temperature (*T_f*) for each measurement. Inset*

shows pictures of the sample in liquid and solid phase during the experiment, the scale bar is 2 mm.

For all the experiments, the temperature (T) of the sample was decreased linearly at the rate of 2 °C min^{-1} until nucleation occurred. The beginning of nucleation was accompanied by a sudden temperature jump to 0 °C due to the latent heat release (**Figure 1c**), after which the sample cooled to the substrate temperature. This frozen sample was then heated back to room temperature to complete a cycle. For the same water sample, 100 such cycles (iterations) were performed under different electric field as shown in **Figure 2a**. Using this experimental data, we generated a "survival curve" (**Figure 2b**), which is defined as the number of the samples frozen at T divided by the total number of samples [32]. The survival curve represents the temperature window in which the water sample froze during the 100 cycles (**Figure 2b**) and the width of this curve highlights the stochastic nature of heterogeneous nucleation. As shown in **Figure 2b**, the presence of the electric field shifted the survival curves to higher freezing temperatures, although the width of the survival curves remains almost the same suggesting that even in the presence of the electric field, the nucleation process was stochastic in nature. From the survival curve, we get T_f, which is defined as the temperature at which on average 50 % of the samples was frozen. Differences in the freezing points obtained from the survival curves with those obtained from the average of 100 freezing cycles are within 0.2 °C, as shown in **Figure S1**. The experimental results clearly show that U elevated T_f (**Figure 2c**) and that in the absence of the electric field, the T_f, was -9.1°C, which increased to -4.9 °C at 45 V ($E = 2.25\times10^6$ V/m).

Voltages higher than 45 V could not be achieved due to limitations of the experimental set-up, hence the thickness d of the PDMS layer was reduced to understand the effect of stronger electric fields. Various samples with d ranging from 20 μm to 1.5 μm were used. Note that the E across the thinner films was in an order of 10^7 V/m, still below the PDMS breakdown strength of 2.5×10^8 V/m [34]. The

effect of the electric field from all the samples is summarized in **Figure 2d**, which shows that the T_f first increases sharply with E, and when E exceeds 6×10^6 V/m, the increase in T_f is only marginal, exhibiting freezing saturation at -3.5 °C. A similar phenomenon has been reported by Carpenter and Bahadur [28] for water droplets (5 µL) where the freezing saturation at -17 °C was found at the critical electric field strength of 2×10^7 V/m. In our case, the freezing saturation temperature was at much higher temperature due to the use of bulk water instead of a water droplet.

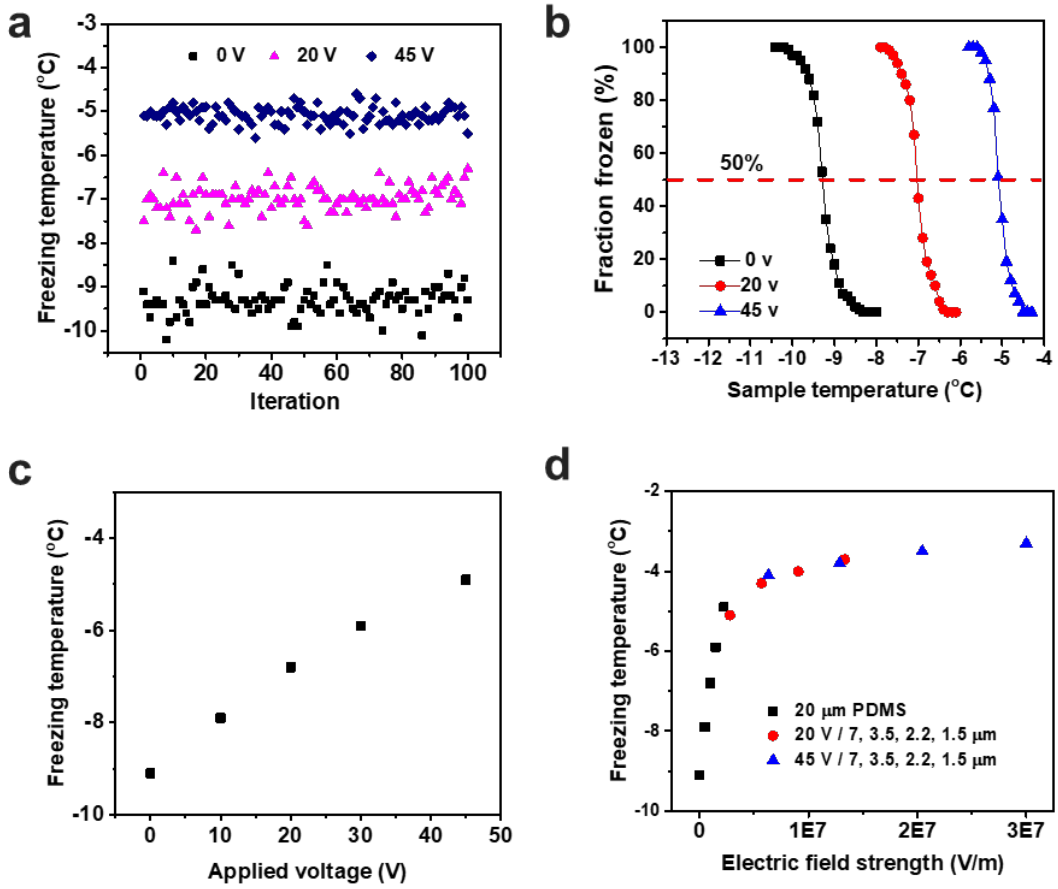

Figure 2. Experimental results. *(a) The freezing temperature T_f as a function of number of cycles (iteration) under three representative voltages on the 20-µm-thickness PDMS surface. (b) Survival curves under three representative voltages on the 20-µm-thickness PDMS surface. The survival curve represents the temperature window in which the water sample froze during the 100 iterations and width of this curve highlights the stochastic nature of heterogeneous nucleation. (c) The freezing temperature*

T_f as a function of applied voltage U on the 20-μm-thickness PDMS surface. (d) The relationship between the freezing temperature T_f and electric field strength, E. Black squares represent results from the 20-μm-thick PDMS surface under different U; red circles and blue triangles represent results from samples where the PDMS thickness was varied from 20 μm to 1.5 μm (from left to right in the figure) under 20-V and 45-V voltage respectively.

Using a simple classical nucleation model, we provide a mechanistic understanding of supercooling under a static electric field. Considering the effect of the substrate on both the nucleation barrier and the transport process, the heterogeneous nucleation rate (J) is given by[35]

$$J = J_0 \exp\left[-\Delta G^* / (k\,T)\right] \tag{1}$$

where J_0 is the prefactor, k is Boltzmann's constant, ΔG^* is the free energy barrier in heterogeneous nucleation,

$$\Delta G^* = \max\left[\Delta G(R)\right] = \max\left[f\left(4\,\pi\,R^2\,\gamma_{iw} - 4/3\,\pi\,R^3\,\Delta G_v\right)\right] \tag{2}$$

where $\Delta G(R)$ is the free energy change associated with the formation of an ice nucleus as a function of the ice nucleus radius R, f is a surface factor that accounts for surface roughness (R_s) and the contact angle of the ice embryo (θ_i) with the substrate, γ_{iw} is the ice-water interfacial tension. $\Delta G_v = H_v\,\Delta T / T_m$ is volume free energy change, H_v is the volumetric latent heat, T_m is the equilibrium melting point, ΔT is the subcooling (T_m - T). Mathematically, ΔG^* is defined by d ΔG (R) /d R = 0, which leads to the following equation

$$\Delta G^* = 16\pi\,\gamma_{iw}^3 T_m^2\,f / 3\,H_v^2\,\Delta T^2 \tag{3}$$

For nucleation under E, previous studies have demonstrated that the free energy of water $\Delta G(R)$, has an additional electrostatic component (ΔG_E) caused by the free energy difference between ice and water[36]

$$\Delta G(R) = f\,[4\,\pi\,R^2\,\gamma_{iw} - 4/3\,\pi\,R^3\,(\Delta G_v + \Delta G_E)] \quad (4)$$

Here ΔG_E can be expressed as

$$\Delta G_E = -1/2\,\varepsilon_0\,\varepsilon_w\,(1 - \varepsilon_i / \varepsilon_w)\,(2 + \varepsilon_i / \varepsilon_w)\,E^2 \quad (5)$$

where ε_0 is the permittivity of vacuum, ε_w and ε_i are dielectric constants of water and ice, respectively. Substituting **Equation (4)** into **Equation (2)** and performing the same mathematical derivation, we can write ΔG^* in a similar form to **Equation (3)**

$$\Delta G^* = 16\pi\,\gamma_{iw}{}^3 T_m{}^2\,f / 3\,H_v{}^2\,(\Delta T + \Delta G_E\,T_m / H_v)^2 \quad (6)$$

Here, ΔT is the supercooling without electric field. The second term in the brackets demonstrates the temperature change due to the electric field and can be defined as

$$\Delta T_E = \Delta G_E\,T_m / H_v \quad (7)$$

For our experiments, the maximum E was 3×10^7 V/m. Under such an electric field, $\Delta G_E = -1.10\times10^4$ J/m^3 (**Equation (5)**) where the values of dielectric constants of water and ice were used from the literature. [37] Inserting ΔG_E and $H_v = 3.34\times10^8$ J/m^3 in **Equation (7)**, ΔT_E is 9.0×10^{-3} °C which is 2-3 orders magnitude smaller than ΔT (more than 2 °C). That means ΔG_E is negligible and hence can be omitted in our case. Similar conclusions have been reached by previous studies [37-38]; especially molecular simulation studies have shown that the field strength required to cause freezing in bulk water should be in the order of 10^9 V/m [39]. Another possible mechanism reported in the literature is that the applied electric field may cause a mechanical perturbation into the liquid, such as in electro-wetting induced liquid spreading [27]. These perturbations in a liquid typically occur as soon as the electric field is turned on. In our experiment, the electric field was applied at the very beginning of the cooling process when the temperature of the liquid was above zero (@10 °C), so any perturbation due to applied electric field should have minimal effect on the supercooling.

So how does the electric field affect ice nucleation? The analysis above has shown that the ΔG_E has little effect on T_f. In **Equation (1)**, according to Fletcher[40], the prefactor J_0 is related with two factors. One is the number of molecules in contact with the substrate. In our cases, the freezing samples are thin liquid films. The electric field did not change the shape of the film and the area of the contacting surface, so the numbers of molecules in contact with the substrate for both cases (with E or not) should be same; the other one is the diffusion activation energy of a water molecule to cross the water/ice interface, which is also not affected by E[33, 40]. Although some studies have demonstrated that the electric field can enhance the translational diffusion of water[41-42], however, in these cases water is confined in sub-nano and nano-spaces, which are quite different from our case. Based on these considerations, we assume J_0 to be constant and hence independent of E. It is possible that under the applied electric field, there is a change in substrate-ice interactions owing to the presence of the electrical double layer near the substrate as reported for water droplets in the literature[37]. These substrate-ice interactions are accounted for in the factor f. To quantify the effect of electric field on f, we carried out systematic measurements of the induction time (τ) as a function of subcooling ΔT by adopting an experimental approach used by Zhang et.al.[8], details of which are provided in the **Experimental Procedures** section. **Figure 3a** shows the experimental data of τ with ΔT under different E. Using correlation $J = 1/\tau V$, where V is the volume of water, we plotted J as a function of ΔT as shown in the **Figure 3b**. By using **Equation (8)**, we need to fit for both J_0 and f

$$\ln J = \ln J_0 - \Omega f / T \Delta T^2 \quad (8)$$

where $\Omega = 16\pi \gamma_{iw}^3 T_m^2 / 3k H_v^2$ is a scaling factor proportional to the nucleation barrier. As mentioned earlier J_0 is independent of E, and since ΔT is related to E, f is a function of E. Hence, we only varied the value of f for fitting the experimental data under electric field. The experimental and fitted results

for J are shown in **Figure 3b**. **Figure 3c** shows the fitted values of f and its variation with E, emphasizing that the f only decreases sharply with E in the beginning and then stays almost constant when E exceeds 6×10^6 V/m.

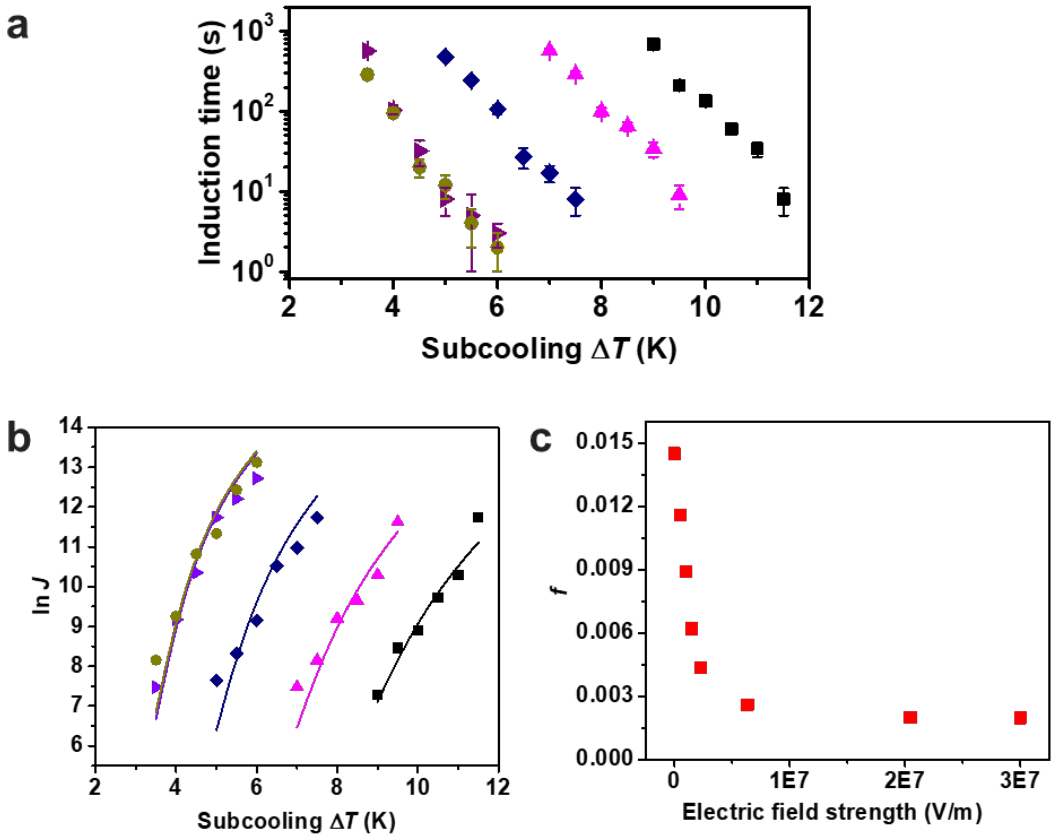

Figure 3. Nucleation model. *a) The experimentally measured induction time τ as a function of subcooling ΔT. b) Experimental and fitted nucleation rate J as a funtion of ΔT. The experimental J can be obtained through J = 1/ τ V, where V is the water volume. J from water freezing on 20-μm PDMS without an electric field (Black square), 20-μm PDMS under 20-V voltage (violet triangle), 20-μm PDMS under 45-V voltage (navy diamond), 7.1-μm PDMS under 45-V voltage (purple right-triangle) and 1.5-μm PDMS under 45-V voltage (yellow circle). (c) Fitted f versus the electric field strength E.*

As mentioned earlier, the factor f accounts for substrate-ice interactions and is governed by the energy [43-44] and geometry of the involved interfaces [45-46]. Owing to substrate-ice interactions, the free energy barrier for heterogeneous nucleation (ΔG) is reduced when compared to that for homogenous

nucleation (ΔG^{homo}) by $f = \Delta G / \Delta G^{homo}$ ($0 < f < 1$). Using classical nucleation theory that assumes that the ice embryo is spherical with a contact angle θ_i (**Figure S2**), f can be expressed as:

$$f = 1/2 + 1/2[(1 - m\,x) / w]^3 + 1/2\,x^3\,\{2 - 3(x - m) / w + [(x - m) / w]^3\} + 3/2\,m\,x^2\,[(x - m) / w - 1] \quad (9)$$

where $w = [1 + x^2 - 2\,x\,m]^{1/2}$, $x = R_s / R_c$, $R_c = 2\,T_m\,\gamma_{iw} / H_v\,\Delta T$ is the critical ice nucleus radius, $m = \cos\theta_i$ and R_s is roughness of the surface. Our atomic force microscopy (AFM) measurement (**Figure S3a**) shows that R_s of the PDMS surface is around 100 nm that is an order of magnitude larger than R_c (4 to 11 nm) at the experimental subcoolings. Thus, f can be simplified as

$$f = (2 + m)\,(1 - m)^2 / 4 \quad (10)$$

From **Equation (10)** we can see f decreases with the increase of m. For ice nucleation, m has a physical meaning of the structural match between the surface and ice. According to Liu et al. [47], m can be expressed as

$$m = (\gamma_{sw} - \gamma_{si}) / \gamma_{iw} = (\gamma_{sw} - \Lambda\,\delta) / \gamma_{iw} \quad (11)$$

where γ_{si} and γ_{sw} are the substrate-ice and substrate-water interfacial energies, respectively, Λ is a constant, $\delta = (a_i - a_s) / a_s$ is the degree of mismatch between ice and the substrate, a_i and a_s are ice and substrate lattice parameters, respectively. Previous studies demonstrated the heterogeneous nucleation is always affected by the structure of the interfacial water adsorption layer, i. e., the transition layer of a few nanometers between the substrate and ice nucleus [27, 48-50]. Other work suggests that ice nucleation rarely occurs directly on the substrate but rather on top of water layers adsorbed on the solid substrate [51-52]. Under this assumption, the δ represents the lattice mismatch between ice and the adsorbed water layer. In addition, many studies have shown that the electric field near the surface can restructure or reorder water molecules in the adsorption layer [53-54]. Using **Equation (11)**, we hypothesize that the

electric field reduces δ, due to the re-ordering of water molecules. The maximum m can be reached when $\delta = 0$, i.e., there is no mismatch, and $m_{max} = \gamma_{sw} / \gamma_{iw}$. This could be the reason why there is a limit for electro-induced freezing on a flat surface.

We wanted to investigate if nano-structuring of the surfaces could affect the freezing saturation. Using a similar electro-freezing platform as shown in **Figure 1a**, we replaced the PDMS coated flat aluminum surface, with a vertically aligned carbon nanotube (CNT) array coated with PDMS (see details in **Experimental Procedures**). The average thickness of the top layer of the PDMS is about 1.5 μm (**Figure 4d**), and the roughness of the PDMS on CNT array is about 1 μm (**Figure S3b**). **Figure 4a – 4d** show the scanning electron microscope (SEM) images of top and cross-sectional views of CNT array before and after coating. The PDMS coating resulted in a collapse of CNTs into bundles as seen in **Figure 4e**, and analysis of the cross-sectional SEM images, revealed the average diameters of CNT bundles lay between 3-5 μm.

We carried out freezing measurements on these CNT-based electro-freezing platforms, and the results are shown in **Figure 4f**. Under no electric field, the freezing point of deionized water on PDMS coated CNT array (PDMS-CNT) was -8.3 °C, which was close to that observed on PDMS-Al (-9.1°C). Although the surface roughness of PDMS-CNT was quite different from that of PDMS-Al, the T_f on these two PDMS surfaces in the absence of electric field was remarkably similar. This signifies that R_s has little effect on T_f when R_s is much larger than R_c. However, under the electric field, the freezing temperature trend for PDMS-CNT was quite different as T_f on PDMS-CNT did not saturate at 6×10^6 V/m and kept increasing until the value reaches to -0.6 °C, which is quite close to the melting point.

In both cases (PDMS-Al and PDMS-CNT), the PDMS surface was in contact with water and hence m should be the same as it reflects the interaction and the structural match between the surface and ice

according to **Equation (11)**. We believe that the change of freezing behavior on PDMS-CNT could be due to the non-uniformity of the electric field caused by heterogeneous distribution of CNT bundles in the sample. As can be seen from **Figure 4e**, the CNTs collapsed into bundles of 3-5 microns diameter. This resulted in a non-uniform distribution of CNTs leading to areas with high density of CNTs and areas without CNTs as shown in the schematic **in Figure 4g**. We believe that this non-uniformity of CNTs in the sample resulted in a non-uniform electric field across the PDMS. It is known that any dielectric (water in our case) when placed in non-uniform electric field, is affected by the volumetric electro-strictive forces, which tend to deform the dielectric and move it to the region of the stronger field [55-56]. This force may generate micro-flows near the substrate, which is a potential driving mechanism for ice nucleation [57]. The reason is that the micro-flow near the surface causes a disturbance into the liquid and increases the possibility of water molecules across the phase boundary between ice and water. It has been reported that these mechanical perturbations (agitation or fluid shear) increases the prefactor J_0 [58-60]. In our case, the prefactor J_0 increased due to the mechanical perturbations caused by a non-uniform electric field. Based on **Equation (1)**, the increase in J_0 resulted in a higher nucleation rate, which could be the reason for near –zero T_f for PDMS-CNT. However, this requires further investigation in the future. We aim to extend this study to carbonaceous materials (graphene, functionalized carbon nanotubes etc..) to understand which kind of a carbon surface can be a good descriptor for ice nucleation under an electric field.[38, 61-64]

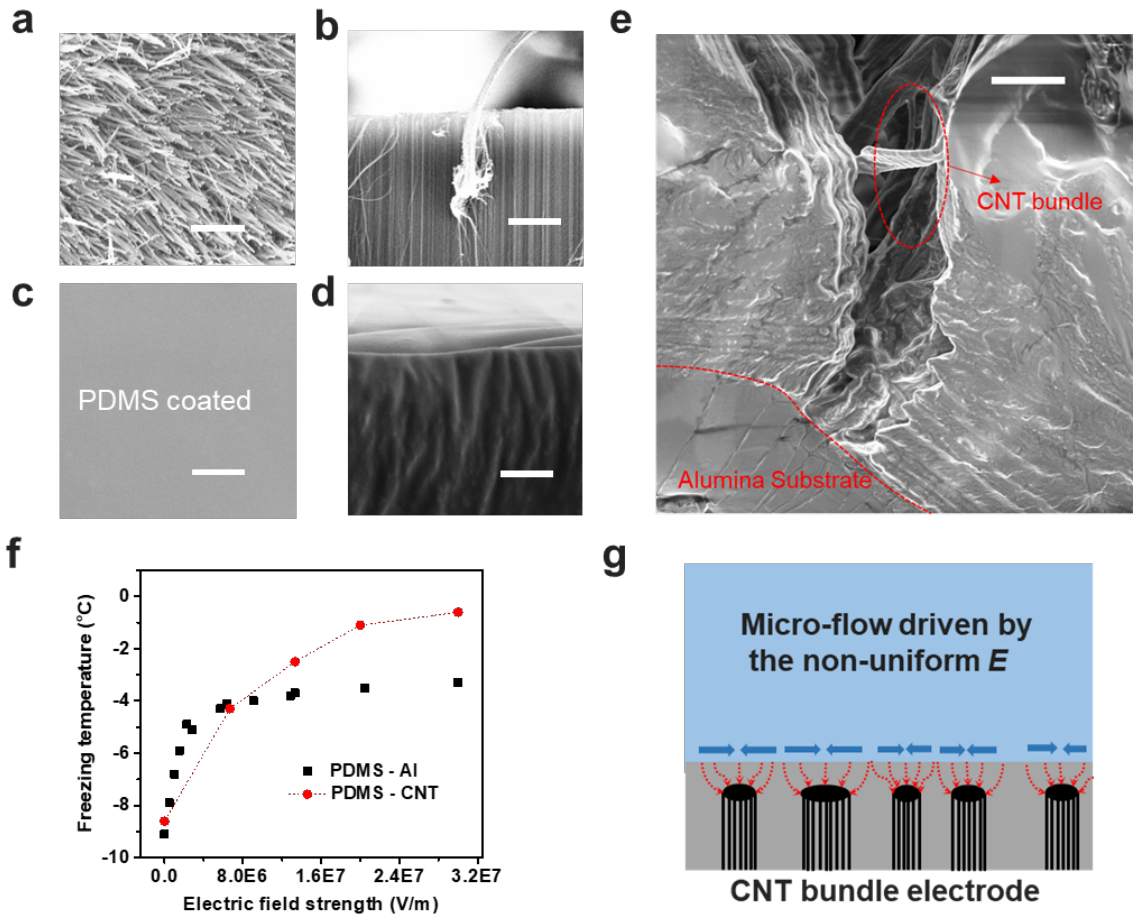

Figure 4. Freezing results on CNT-PDMS composite. *(a) Top-view (the scale bar is 2 μm) and (b) side-view (the scale bar is 20 μm) of CNT array before coating. (c) Top-view (the scale bar is 2 μm) and (d) side-view (the scale bar is 5 μm) of CNT array after coating. (e) Side view SEM shows the CNT bundles on the alumina substrate, circled by dash line. The scale bar is 30 μm. (f) The freezing temperature* T_f *versus electric field strength E on PDMS – CNT (red circular points). The results on PDMS - Al (black square points) are also shown for comparison. (g) Possible micro-scale mechanisms. The electric field strength is not uniform at the solid-liquid interface, which may cause micro-flow near the surface and facilitate ice nucleation.*

A key element missing in our work and in the literature on electro freezing is a molecular level understanding of the interfacial mechanisms underlying nucleation and subsequent ice formation. Here it is important to be able to probe the hydrogen bond dynamics occurring between the electrified

interface and bulk liquid water [65]. The IR and THz region of the water spectrum is highly affected by its hydrogen-bonding environment and is thus an excellent probe for the effect of electric field on its properties. Attenuated Total Reflection Spectroscopy (ATR), which allows direct insight into the interface and the double layer, could be readily applied to our experimental platform. For our future work, we plan to design chip based ATR devices coupled to microfluidics, electrodes and heating/cooling elements which could be transported between traditional Fourier Transform Infrared Spectrometers and broadband THZ and IR lasers to provide a comprehensive picture of the vibrational spectroscopy of water [66]. The Si based ATR chip can also be functionalized and impregnated with novel nano-structured electrodes to probe local electric fields. We note that there is an extensive literature on the application of molecular dynamic simulations awaiting experimental verification and our proposed methods and future work will go some way in this direction.

CONCLUSION

In summary, we systematically investigated external electric-field effects on heterogeneous nucleation in bulk water. Increase of the freezing temperature has been found below a critical electric field strength, above which the freezing temperature does not change much. The phenomena may be attributed to the change of ice contact angle on the substrate under a static electric field. We also found the saturation of the freezing point can be eliminated by using a nano-structured electrode. These observations shed new light on the control of ice nucleation and has the potential for extended applications in both anti-icing and efficient ice-production.

EXPERIMENTAL PROCEDURES

Materials. Vinyl-terminated PDMS (v-PDMS, M_w = 95 kg/mol), hydride-terminated PDMS (h-PDMS, M_w = 1.3 kg/mol) and trimethyl-terminated PDMS (t-PDMS, M_w = 28 kg/mol) were purchased from

Sigma-Aldrich.

PDMS gel layer fabrication. The PDMS gel was synthesized via hydrosilylation of v-PDMS with h-PDMS.[67-68] Briefly, the v-PDMS and h-PDMS in a ratio of 10:1 were mixed with the 50% weight of t-PDMS. The mixture was then degassed in a vacuum oven for 30 mins and spin coated onto the aluminum surface as an electrode. The thickness, *d*, was controlled by the coating time and spinning speed. Finally, the coated electrode was cross-linked in an oven at 70 °C for 24 hours.

PDMS-CNT composite fabrication. CNT arrays were grown on Si substrates by CVD using an automated wafer-scale CVD system for carbon-based material growth (Aixtron Black Magic Pro). A 10-nm thick Al2O3 layer and a 2-nm thick Fe layer were deposited on the Si wafer by e-beam evaporation. MWCNT arrays were grown in the tube furnace at 770 °C using ethylene as the carbon source. CNT diameters were 18 nm and lengths were 70 - 100 μm. After the CNT growth, an aluminum tape was placed on the top of the CNT array and the CNT array was then peeled off from the Si wafer onto aluminum tape. The PDMS gel was then drop casted onto the CNT array and cured at 70 °C for 24 hours. The schematic in **Figure S4** shows the fabrication process.

Surface characterization. Surface morphology was observed with a scanning electronic microscope (SEM), and the roughness was measured using an atomic force microscope (AFM). The thickness of PDMS on aluminum was measured by using an optical profiler, and the thickness of PDMS on top of CNT array was measured from the cross-sectional SEM images of PDMS coated CNT samples. Each thickness is an average thickness of 5 different points of the sample.

Freezing measurement. The experiments were conducted in an environment with constant temperature of 20 °C and relative humidity of 20 %, respectively. To avoid the effect of airflow, the freezing sample was placed inside a glass chamber, whose size is slightly larger than that of the vial. In case of

evaporation of liquid and condensation of the vapor in the chamber, the freezing sample was covered by a thin oil film. Note that the film is still transparent allowing the camera to capture the ice nucleation process. The cooling surface temperature was controlled by a Peltier cooling system with a water circulation and temperature controller. A thermocouple probe with a resolution of 0.1 °C was first coated with a PDMS gel layer to avoid nucleation on itself, and then inserted into the liquid and kept contact with the bottom surface to monitor the temperature of liquid/ice. During the experiment, the temperature difference between the cooling surface and vessel bottom surface was no more than 0.2 °C.

Nucleation rate and induction time measurement. Figure S5 describes the methodology to measure the induction time. The nucleation surface was cooled rapidly to a constant temperature below the melting point (surface subcooling), after a period of induction, the onset of nucleation occurs with a sudden temperature increase. Using this method, induction times under different subcooling were recorded [64, 69]. In all experiments, the duration of rapid cooling is far less than the induction time and its effect on nucleation can be omitted. Every induction time test was repeated at least 10 times, and the average value was applied to further data processing. Based on the measured data, we estimate the average nucleation rate to be $J = 1 / \tau V_0$, where V_0 is the volume of the freezing sample.

TOC GRAPHIC

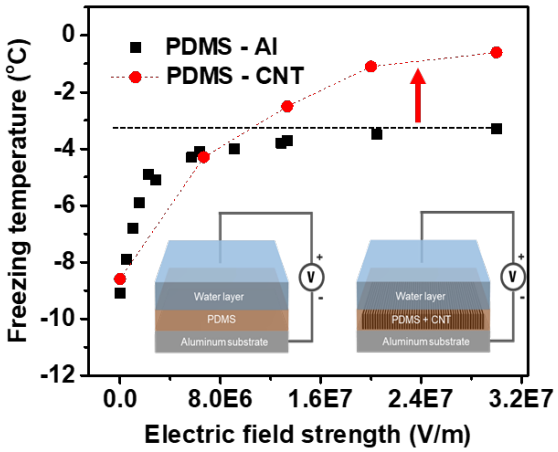

ASSOCIATED CONTENT

Supporting Information

Verification of the precision of experimental freezing points, Schematic description of ice embryo sitting on a rough surface, AFM images of the PDMS and PDMS-CNT surfaces, schematic description of the fabrication process of PDMS-CNT composite, and the temperature history during the measurement of the induction time (PDF).

ACKNOWLEDGMENTS

This work was supported by the Laboratory Directed Research and Development Program (LDRD) at Lawrence Berkeley National Laboratory under contract # DE-AC02-05CH11231. MA acknowledges the support of the Director, Office of Science, Office of Basic Energy Sciences, of the U.S. DOE under Contract No. DE-AC02-05CH11231, through the Condensed Phase, Interfaces, and Molecular Sciences Program.

REFERENCE

(1) Lv, J.; Song, Y.; Jiang, L.; Wang, J. Bio-Inspired Strategies for Anti-Icing. *ACS Nano* **2014,** *8* (4), 3152-3169, DOI: 10.1021/nn406522n.

(2) Kreder, M. J.; Alvarenga, J.; Kim, P.; Aizenberg, J. Design of Anti-icing Surfaces: Smooth, Textured or

Slippery? *Nature Reviews Materials* **2016,** *1*, 15003, DOI: 10.1038/natrevmats.2015.3.
(3) Golovin, K.; Kobaku, S. P. R.; Lee, D. H.; DiLoreto, E. T.; Mabry, J. M.; Tuteja, A. Designing Durable Icephobic Surfaces. *Science Advances* **2016,** *2* (3), e1501496, DOI: 10.1126/sciadv.1501496.
(4) Yau, Y. H.; Rismanchi, B. A Review on Cool Thermal Storage Technologies and Operating Strategies. *Renewable and Sustainable Energy Reviews* **2012,** *16* (1), 787-797, DOI: https://doi.org/10.1016/j.rser.2011.09.004.
(5) Li, G.; Zheng, X. Thermal Energy Storage System Integration Forms for a Sustainable Future. *Renewable and Sustainable Energy Reviews* **2016,** *62*, 736-757, DOI: https://doi.org/10.1016/j.rser.2016.04.076.
(6) Dalvi-Isfahan, M.; Hamdami, N.; Xanthakis, E.; Le-Bail, A. Review on the Control of Ice Nucleation by Ultrasound Waves, Electric and Magnetic fields. *Journal of Food Engineering* **2017,** *195*, 222-234, DOI: https://doi.org/10.1016/j.jfoodeng.2016.10.001.
(7) Kalista, B.; Shin, H.; Cho, J.; Jang, A. Current Development and Future Prospect Review of Freeze Desalination. *Desalination* **2018,** *447*, 167-181, DOI: https://doi.org/10.1016/j.desal.2018.09.009.
(8) Zhang, Z.; Liu, X.-Y. Control of Ice Nucleation: Freezing and Antifreeze Strategies. *Chemical Society Reviews* **2018**, *47*, 7116-7139, DOI: 10.1039/C8CS00626A.
(9) Lo, C.-W.; Sahoo, V.; Lu, M.-C. Control of Ice Formation. *ACS Nano* **2017,** *11* (3), 2665-2674, DOI: 10.1021/acsnano.6b07348.
(10) Koop, T.; Luo, B.; Tsias, A.; Peter, T. Water Activity as the Determinant for Homogeneous Ice Nucleation in Aqueous Solutions. *Nature* **2000,** *406*, 611-614, DOI: 10.1038/35020537.
(11) He, Z.; Liu, K.; Wang, J. Bioinspired Materials for Controlling Ice Nucleation, Growth, and Recrystallization. *Accounts of chemical research* **2018,** *51* (5), 1082-1091.
(12) Sellberg, J. A.; Huang, C.; McQueen, T. A.; Loh, N. D.; Laksmono, H.; Schlesinger, D.; Sierra, R. G.; Nordlund, D.; Hampton, C. Y.; Starodub, D.; DePonte, D. P.; Beye, M.; Chen, C.; Martin, A. V.; Barty, A.; Wikfeldt, K. T.; Weiss, T. M.; Caronna, C.; Feldkamp, J.; Skinner, L. B.; Seibert, M. M.; Messerschmidt, M.; Williams, G. J.; Boutet, S.; Pettersson, L. G. M.; Bogan, M. J.; Nilsson, A. Ultrafast X-ray Probing of Water Structure below the Homogeneous Ice Nucleation Temperature. *Nature* **2014,** *510*, 381-384, DOI: 10.1038/nature13266.
(13) Naullage, P. M.; Qiu, Y.; Molinero, V. What Controls the Limit of Supercooling and Superheating of Pinned Ice Surfaces? *The Journal of Physical Chemistry Letters* **2018,** *9* (7), 1712-1720, DOI: 10.1021/acs.jpclett.8b00300.
(14) Bigg, E. K. The Supercooling of Water. *Proceedings of the Physical Society. Section B* **1953,** *66* (8), 688-694.
(15) Moore, E. B.; Molinero, V. Structural Transformation in Supercooled Water Controls the Crystallization Rate of Ice. *Nature* **2011,** *479*, 506-508, DOI: 10.1038/nature10586.
(16) Mossop, S. The Freezing of Supercooled Water. *Proceedings of the Physical Society. Section B* **1955,** *68* (4), 193-208.
(17) Woo, M. W.; Mujumdar, A. S. Effects of Electric and Magnetic Field on Freezing and Possible Relevance in Freeze Drying. *Drying Technology* **2010,** *28* (4), 433-443, DOI: 10.1080/07373930903202077.
(18) Gibbs, A.; Charman, M.; Schwarzacher, W.; Rust, A. C. Immersion Freezing of Supercooled Water Drops Containing Glassy Volcanic Ash Particles. *GeoResJ* **2015,** *7*, 66-69, DOI: https://doi.org/10.1016/j.grj.2015.06.002.
(19) Okawa, S.; Saito, A.; Minami, R. The Solidification Phenomenon of the Supercooled Water Containing Solid Particles. *International Journal of Refrigeration* **2001,** *24* (1), 108-117, DOI: https://doi.org/10.1016/S0140-7007(00)00060-8.
(20) Jha, P. K.; Sadot, M.; Vino, S. A.; Jury, V.; Curet-Ploquin, S.; Rouaud, O.; Havet, M.; Le-Bail, A. A Review on Effect of DC Voltage on Crystallization Process in Food Systems. *Innovative Food Science & Emerging*

Technologies **2017,** *42*, 204-219, DOI: https://doi.org/10.1016/j.ifset.2017.06.002.
(21) Ehre, D.; Lavert, E.; Lahav, M.; Lubomirsky, I. Water Freezes Differently on Positively and Negatively Charged Surfaces of Pyroelectric Materials. *Science* **2010,** *327* (5966), 672-675, DOI: 10.1126/science.1178085.
(22) Yang, H.; Ma, C.; Li, K.; Liu, K.; Loznik, M.; Teeuwen, R.; van Hest, J. C. M.; Zhou, X.; Herrmann, A.; Wang, J. Tuning Ice Nucleation with Supercharged Polypeptides. *Advanced Materials* **2016,** *28* (25), 5008-5012, DOI: doi:10.1002/adma.201600496.
(23) Wildeman, S.; Sterl, S.; Sun, C.; Lohse, D. Fast Dynamics of Water Droplets Freezing from the Outside In. *Physical Review Letters* **2017,** *118* (8), 084101, DOI: 10.1103/PhysRevLett.118.084101.
(24) Yang, F.; Shaw, R. A.; Gurganus, C. W.; Chong, S. K.; Yap, Y. K. Ice Nucleation at the Contact Line Triggered by Transient Electrowetting Fields. *Applied Physics Letters* **2015,** *107* (26), 264101, DOI: 10.1063/1.4938749.
(25) Orlowska, M.; Havet, M.; Le-Bail, A. Controlled Ice Nucleation under High Voltage DC Electrostatic Field Conditions. *Food Research International* **2009,** *42* (7), 879-884, DOI: https://doi.org/10.1016/j.foodres.2009.03.015.
(26) Wei, S.; Xiaobin, X.; Hong, Z.; Chuanxiang, X. Effects of Dipole Polarization of Water Molecules on Ice Formation under an Electrostatic Field. *Cryobiology* **2008,** *56* (1), 93-99, DOI: https://doi.org/10.1016/j.cryobiol.2007.10.173.
(27) Wu, S.; He, Z.; Zang, J.; Jin, S.; Wang, Z.; Wang, J.; Yao, Y.; Wang, J. Heterogeneous Ice Nucleation Correlates with Bulk-like Interfacial Water. *Science advances* **2019,** *5* (4), eaat9825.
(28) Carpenter, K.; Bahadur, V. Electrofreezing of Water Droplets under Electrowetting Fields. *Langmuir* **2015,** *31* (7), 2243-2248, DOI: 10.1021/la504792n.
(29) Niedermeier, D.; Shaw, R.; Hartmann, S.; Wex, H.; Clauss, T.; Voigtländer, J.; Stratmann, F. Heterogeneous Ice Nucleation: Exploring the Transition from Stochastic to Singular Freezing Behavior. *Atmospheric Chemistry and Physics* **2011,** *11* (16), 8767-8775.
(30) Leonard, J.; Im, J. S. Stochastic Modeling of Solid Nucleation in Supercooled Liquids. *Applied Physics Letters* **2001,** *78* (22), 3454-3456.
(31) Vali, G. Interpretation of Freezing Nucleation Experiments: Singular and Stochastic; Sites and Surfaces. *Atmospheric Chemistry and Physics* **2014,** *14* (11), 5271-5294.
(32) Heneghan, A.; Wilson, P.; Haymet, A. Heterogeneous Nucleation of Supercooled Water, and the Effect of an Added Catalyst. *Proceedings of the National Academy of Sciences* **2002,** *99* (15), 9631-9634.
(33) Seeley, L.; Seidler, G. Two-dimensional Nucleation of Ice from Supercooled Water. *Physical Review Letters* **2001,** *87* (5), 055702.
(34) Gerratt, A. P.; Bergbreiter, S. Dielectric Breakdown of PDMS Thin Films. *Journal of Micromechanics and Microengineering* **2013,** *23* (6), 067001.
(35) Jung, S.; Tiwari, M. K.; Doan, N. V.; Poulikakos, D. Mechanism of Supercooled Droplet Freezing on Surfaces. *Nature Communications* **2012,** *3*, 615, DOI: 10.1038/ncomms1630.
(36) Acharya, P. V.; Bahadur, V. Fundamental Interfacial Mechanisms Underlying Electrofreezing. *Advances in Colloid and Interface Science* **2018,** *251*, 26-43, DOI: https://doi.org/10.1016/j.cis.2017.12.003.
(37) Zhang, X.-X.; Li, X.-H.; Chen, M. Role of the Electric Double Layer in the Ice Nucleation of Water Droplets under an Electric Field. *Atmospheric Research* **2016,** *178-179*, 150-154, DOI: https://doi.org/10.1016/j.atmosres.2016.04.001.
(38) Whale, T. F.; Rosillo-Lopez, M.; Murray, B. J.; Salzmann, C. G. Ice Nucleation Properties of Oxidized Carbon Nanomaterials. *The Journal of Physical Chemistry Letters* **2015,** *6* (15), 3012-3016, DOI: 10.1021/acs.jpclett.5b01096.
(39) Yan, J. Y.; Patey, G. N. Heterogeneous Ice Nucleation Induced by Electric Fields. *The Journal of Physical*

Chemistry Letters **2011,** *2* (20), 2555-2559, DOI: 10.1021/jz201113m.
(40) Fletcher, N. H. The Physics of Rainclouds, Cambridge University Press: 2011.
(41) Diallo, S.; Mamontov, E.; Nobuo, W.; Inagaki, S.; Fukushima, Y. Enhanced Translational Diffusion of Confined Water under Electric Field. *Physical Review E* **2012,** *86* (2), 021506.
(42) Fuchs, E. C.; Bitschnau, B.; Wexler, A. D.; Woisetschläger, J.; Freund, F. T. A Quasi-elastic Neutron Scattering Study of the Dynamics of Electrically Constrained Water. *The Journal of Physical Chemistry B* **2015,** *119* (52), 15892-15900.
(43) Zhang, Y.; Anim-Danso, E.; Bekele, S.; Dhinojwala, A. Effect of Surface Energy on Freezing Temperature of Water. *ACS Applied Materials & Interfaces* **2016,** *8* (27), 17583-17590, DOI: 10.1021/acsami.6b02094.
(44) Li, C.; Gao, X.; Li, Z. Roles of Surface Energy and Temperature in Heterogeneous Ice Nucleation. *The Journal of Physical Chemistry C* **2017,** *121* (21), 11552-11559, DOI: 10.1021/acs.jpcc.7b02848.
(45) Fitzner, M.; Sosso, G. C.; Cox, S. J.; Michaelides, A. The Many Faces of Heterogeneous Ice Nucleation: Interplay Between Surface Morphology and Hydrophobicity. *Journal of the American Chemical Society* **2015,** *137* (42), 13658-13669, DOI: 10.1021/jacs.5b08748.
(46) Qiu, Y.; Odendahl, N.; Hudait, A.; Mason, R.; Bertram, A. K.; Paesani, F.; DeMott, P. J.; Molinero, V. Ice Nucleation Efficiency of Hydroxylated Organic Surfaces Is Controlled by Their Structural Fluctuations and Mismatch to Ice. *Journal of the American Chemical Society* **2017,** *139* (8), 3052-3064, DOI: 10.1021/jacs.6b12210.
(47) Liu, X. Y. Interfacial Effect of Molecules on Nucleation Kinetics. *The Journal of Physical Chemistry B* **2001,** *105* (47), 11550-11558, DOI: 10.1021/jp010671z.
(48) Lupi, L.; Molinero, V. Does Hydrophilicity of Carbon Particles Improve Their Ice Nucleation Ability? *The Journal of Physical Chemistry A* **2014,** *118* (35), 7330-7337, DOI: 10.1021/jp4118375.
(49) Lupi, L.; Hudait, A.; Molinero, V. Heterogeneous Nucleation of Ice on Carbon Surfaces. *Journal of the American Chemical Society* **2014,** *136* (8), 3156-3164, DOI: 10.1021/ja411507a.
(50) Yeh, I. C.; Berkowitz, M. L. Structure and Dynamics of Water at Water|Pt Interface as Seen by Molecular Dynamics Computer Simulation. *Journal of Electroanalytical Chemistry* **1998,** *450* (2), 313-325, DOI: https://doi.org/10.1016/S0022-0728(97)00654-2.
(51) Pruppacher, H. Electrofreezing of Supercooled water. *Pure and Applied Geophysics* **1973,** *104* (1), 623-634.
(52) Evans, L. In *The role of the adsorbed layer in ice nucleation*, Preprint Conf. Cloud Physics, Am. Meteor. Soc., Fort Collins, 1970.
(53) Xia, X.; Berkowitz, M. L. Electric-Field Induced Restructuring of Water at a Platinum-Water Interface: A Molecular Dynamics Computer Simulation. *Physical Review Letters* **1995,** *74* (16), 3193-3196, DOI: 10.1103/PhysRevLett.74.3193.
(54) Toney, M. F.; Howard, J. N.; Richer, J.; Borges, G. L.; Gordon, J. G.; Melroy, O. R.; Wiesler, D. G.; Yee, D.; Sorensen, L. B. Voltage-dependent Ordering of Water Molecules at an Electrode–electrolyte Interface. *Nature* **1994,** *368* (6470), 444-446, DOI: 10.1038/368444a0.
(55) Salipante, P. F.; Vlahovska, P. M. Electrohydrodynamics of Drops in Strong Uniform Dc Electric Fields. *Physics of Fluids* **2010,** *22* (11), 112110.
(56) Shneider, M. N.; Pekker, M. Dielectric Fluid in Inhomogeneous Pulsed Electric Field. *Physical Review E* **2013,** *87* (4), 043004.
(57) Saville, D. Electrohydrodynamics: the Taylor-Melcher Leaky Dielectric Model. *Annual review of fluid mechanics* **1997,** *29* (1), 27-64.
(58) Liu, J.; Rasmuson, Å. C. Influence of Agitation and Fluid Shear on Primary Nucleation in Solution. *Crystal growth & design* **2013,** *13* (10), 4385-4394.

(59) Forsyth, C.; Mulheran, P. A.; Forsyth, C.; Haw, M. D.; Burns, I. S.; Sefcik, J. Influence of Controlled Fluid Shear on Nucleation Rates in Glycine Aqueous Solutions. *Crystal Growth & Design* **2015,** *15* (1), 94-102.
(60) Forsyth, C.; Burns, I. S.; Mulheran, P. A.; Sefcik, J. Scaling of Glycine Nucleation Kinetics with Shear Rate and Glass–liquid Interfacial Area. *Crystal Growth & Design* **2016,** *16* (1), 136-144.
(61) Häusler, T.; Gebhardt, P.; Iglesias, D.; Rameshan, C.; Marchesan, S.; Eder, D.; Grothe, H. Ice Nucleation Activity of Graphene and Graphene Oxides. *The Journal of Physical Chemistry C* **2018,** *122* (15), 8182-8190, DOI: 10.1021/acs.jpcc.7b10675.
(62) Cabriolu, R.; Li, T. Ice Nucleation on Carbon Surface Supports the Classical Theory for Heterogeneous Nucleation. *Physical Review E* **2015,** *91* (5), 052402, DOI: 10.1103/PhysRevE.91.052402.
(63) Ikhenazene, R.; Pirim, C.; Noble, J. A.; Irimiea, C.; Carpentier, Y.; Ortega, I. K.; Ouf, F.-X.; Focsa, C.; Chazallon, B. Ice Nucleation Activities of Carbon-Bearing Materials in Deposition Mode: From Graphite to Airplane Soot Surrogates. *The Journal of Physical Chemistry C* **2020,** *124* (1), 489-503, DOI: 10.1021/acs.jpcc.9b08715.
(64) Xue, H.; Lu, Y.; Geng, H.; Dong, B.; Wu, S.; Fan, Q.; Zhang, Z.; Li, X.; Zhou, X.; Wang, J. Hydroxyl Groups on the Graphene Surfaces Facilitate Ice Nucleation. *The Journal of Physical Chemistry Letters* **2019,** *10* (10), 2458-2462, DOI: 10.1021/acs.jpclett.9b01033.
(65) Perakis, F.; De Marco, L.; Shalit, A.; Tang, F.; Kann, Z. R.; Kühne, T. D.; Torre, R.; Bonn, M.; Nagata, Y. Vibrational Spectroscopy and Dynamics of Water. *Chemical reviews* **2016,** *116* (13), 7590-7607.
(66) Morhart, T. A.; Read, S. T.; Wells, G.; Jacobs, M.; Rosendahl, S. M.; Achenbach, S.; Burgess, I. J. Micromachined Multigroove Silicon ATR FT-IR Internal Reflection Elements for Chemical Imaging of Microfluidic Devices. *Analytical Methods* **2019,** *11* (45), 5776-5783.
(67) Beemer, D. L.; Wang, W.; Kota, A. K. Durable Gels with Ultra-low Adhesion to Ice. *Journal of Materials Chemistry A* **2016,** *4* (47), 18253-18258, DOI: 10.1039/C6TA07262C.
(68) Liu, Y.; Ma, L.; Wang, W.; Kota, A. K.; Hu, H. An Experimental Study on Soft PDMS Materials for Aircraft Icing Mitigation. *Applied Surface Science* **2018,** *447*, 599-609, DOI: https://doi.org/10.1016/j.apsusc.2018.04.032.
(69) Tourkine, P.; Le Merrer, M.; Quéré, D. Delayed Freezing on Water Repellent Materials. *Langmuir* **2009,** *25* (13), 7214-7216.

Supplementary Information

Water Freezes at Near-zero Temperatures Using Carbon Nanotube Based Electrodes under Static Electric Fields

Zhi Huang[1], Sumanjeet Kaur[1,*], Musahid Ahmed[2] and Ravi Prasher[1,3,*]

[1]Energy Storage and Distributed Resources Division, Lawrence Berkeley National Laboratory, Berkeley, CA, USA.

[2]Chemical Sciences Division, Lawrence Berkeley National Laboratory, Berkeley, CA, USA.

[3]Department of Mechanical Engineeing, University of California, Berkeley, Berkeley, CA, USA.

*Corresponding to skaur1@lbl.gov and rsprasher@lbl.gov.

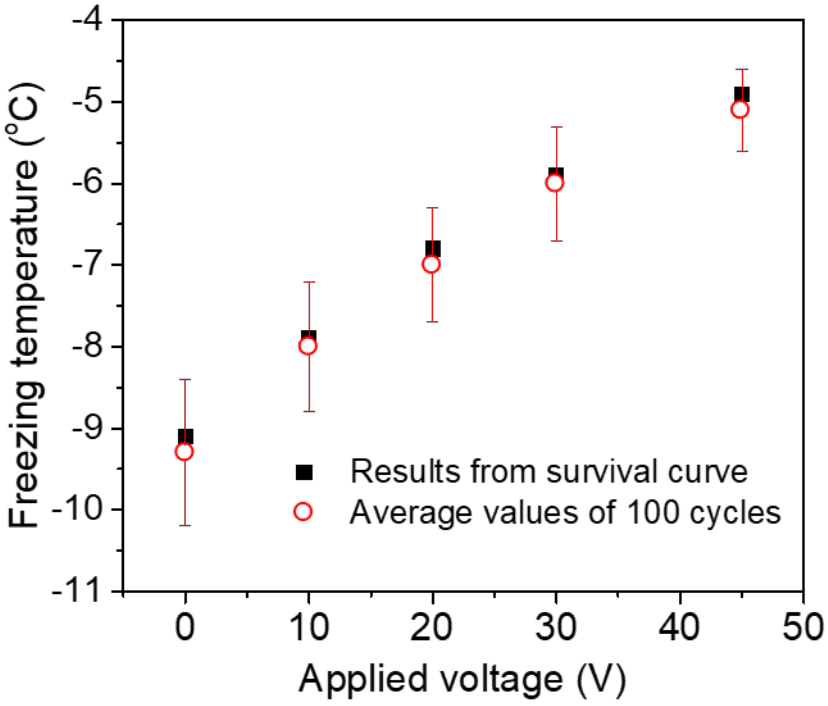

Figure S1. Comparison between the freezing temperatures obtained from the survival curve and the average values of 100 cycle experiments. The differences between them are within 0.2 K.

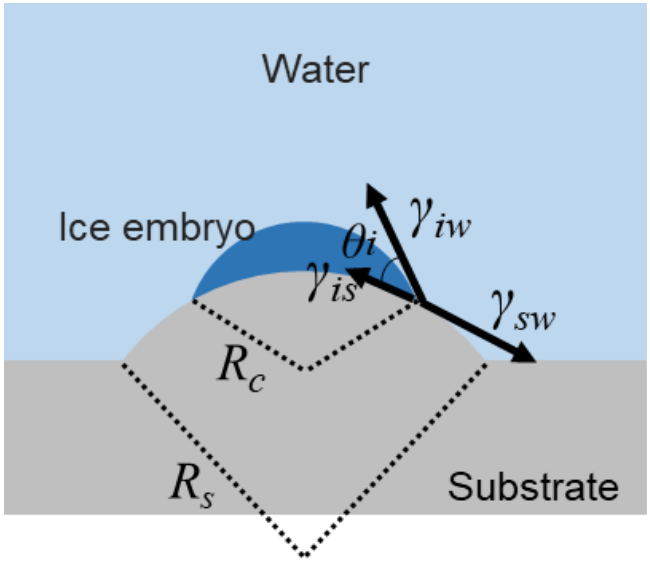

Figure S2. Schematic illustration of Ice nucleation on a substrate with a roughness R_s (the curvature of the surface). The ice embryo is assumed to be in a spherical-cap shape with a curvature radius R_c. θ_i is the contact angle between the ice embryo and the substrate and determined by the interfacial tensions of ice-substrate (γ_{is}), water-substrate (γ_{sw}) and ice-water (γ_{iw}), $\cos \theta_i = (\gamma_{sw} - \gamma_{is}) / \gamma_{iw}$.

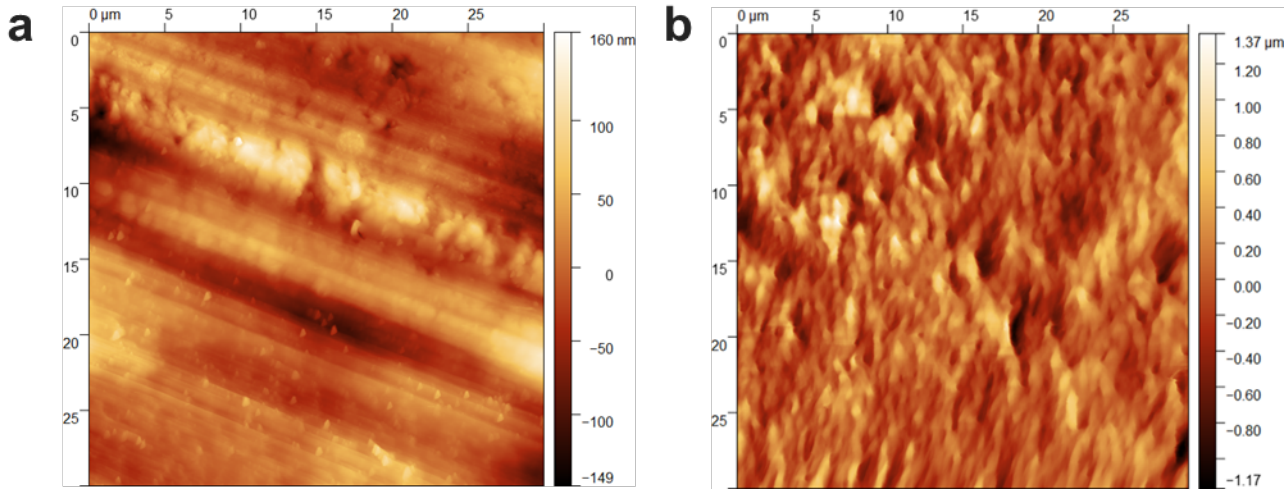

Figure S3. The AFM images of PDMS-Al (a) and PDMS-CNT surfaces (b) in contact with the water. The roughness of surface (a) and surface (b) is about 100 nm and 1 µm, respectively.

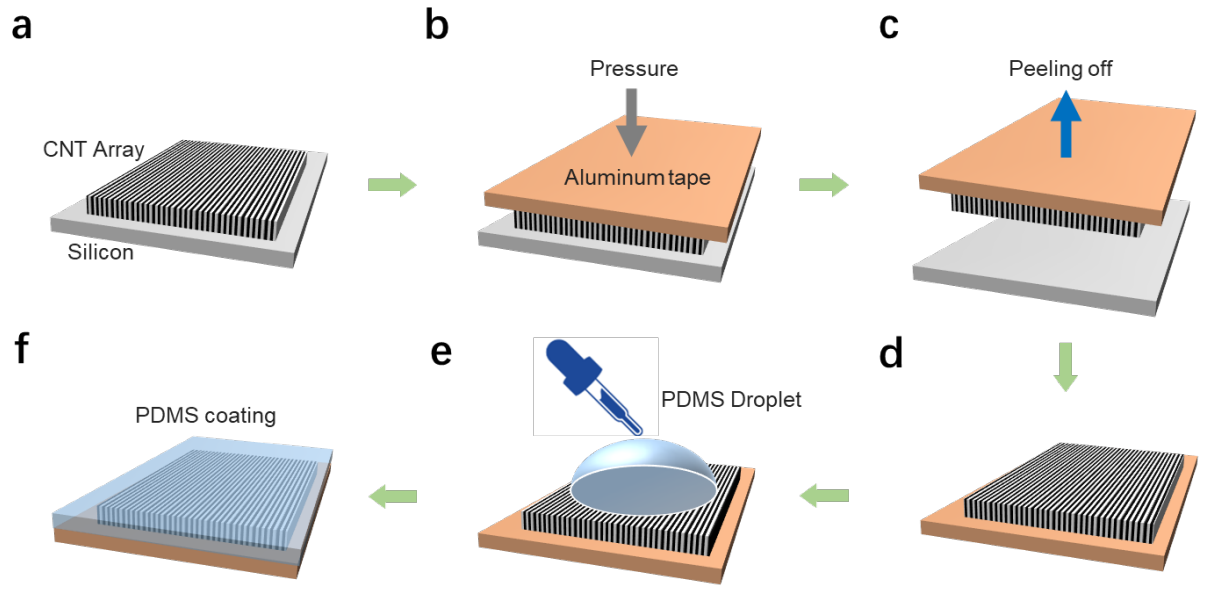

Figure S4. The fabrication process of PDMS-CNT composite. CNT arrays were grown on Si substrates by a chemical vapor deposition method (CVD) (a). After the CNT growth, an aluminum tape was placed on the top of the CNT array (b) and the CNT array was then peeled off from the Si wafer onto aluminum tape (c, d). The PDMS gel was then drop casted onto the CNT array (e) and cured at 70 ºC for 24 hours (f).

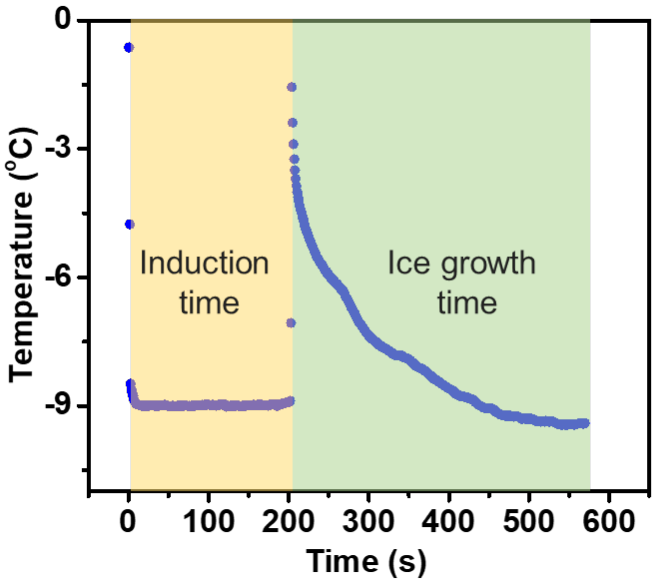

Figure S5. Temperature history during the measurement of the induction time. The nucleation surface was cooled rapidly to a constant temperature below the melting point (surface subcooling), after a period of induction, the onset of nucleation occurs with a sudden temperature increase.

.